Fermionic Superfluidity with Imbalanced Spin Populations

Martin W. Zwierlein,* André Schirotzek, Christian H. Schunck, Wolfgang Ketterle

We established superfluidity in a two-state mixture of ultracold fermionic atoms with imbalanced state populations. This study relates to the long-standing debate about the nature of the superfluid state in Fermi systems. Indicators for superfluidity were condensates of fermion pairs and vortices in rotating clouds. For strong interactions, near a Feshbach resonance, superfluidity was observed for a broad range of population imbalances. We mapped out the superfluid regime as a function of interaction strength and population imbalance and characterized the quantum phase transition to the normal state, known as the Pauli limit of superfluidity.

Fermionic superfluidity, whether it occurs in superconductors, helium-3, or inside a neutron star, requires pairing of fermions, particles with half-integer spin. In an equal mixture of two states of fermions ("spin up" and "spin down"), pairing can be complete and the entire system will become superfluid. When the two populations of fermions are unequal, however, not every particle can find a partner, raising the question of whether superfluidity can persist in response to such a population imbalance. This problem arises in many different fields of physics—for example, in the study of superfluidity of quarks in the dense matter of the early universe, where charge neutrality and differing masses impose unequal quark densities. In superconductors, an applied magnetic field could in principle imbalance the densities of spin up and spin down electrons. As first discussed by Clogston in 1962 (*1*), there exists an upper limit for this magnetic field, beyond which superconductivity with equal spin densities will break down. Fulde and Ferrell (*2*), and independently Larkin and Ovchinnikov (*3*), proposed a more stable configuration of the superconductor that allows for unequal densities, the FFLO or LOFF state containing nonzero-momentum Cooper pairs. The true ground state of imbalanced fermionic superfluids has been the subject of debate for decades (*4*, *5*), and experimental studies are highly desirable. However, superconductors are charged fermionic superfluids, and imbalancing the electron densities by applying magnetic fields is hindered by the Meissner effect. The fields are either fully shielded from the superconductor, or they enter in the form of quantized flux lines or vortices. Only in special materials can these effects be suppressed, such as in heavy-fermion superconductors (*6*–*8*) or in quasi–two-dimensional (2D) organic superconductors (*6*). In the neutral superfluid helium-3, one can mismatch the Fermi surfaces by a magnetic field and thus destroy interspin pairing. However, superfluidity persists due to (p-wave) pairing between equal spins (*9*).

Department of Physics, Massachusetts Institute of Technology (MIT)–Harvard Center for Ultracold Atoms, and Research Laboratory of Electronics, MIT, Cambridge, MA 02139, USA.

*To whom correspondence should be addressed. E-mail: zwierlei@mit.edu

Fermionic superfluids of atom pairs. The recently discovered fermionic superfluids in ultracold atomic gases (*10*–*19*) provide an exciting new possibility of exploring unequal mixtures of fermions, because populations in two hyperfine states of the fermionic atom can be freely chosen. In addition, the (s-wave) interactions between two atoms in different states and the binding energy of atom pairs can be tuned via Feshbach resonances. In equal mixtures of fermions, this tunability gives access to the crossover from a Bose-Einstein Condensate (BEC) of molecules to a Bardeen-Cooper-Schrieffer (BCS) superfluid of loosely bound pairs (*13*–*19*). At zero temperature, this crossover is smooth (*20*–*22*), the system stays

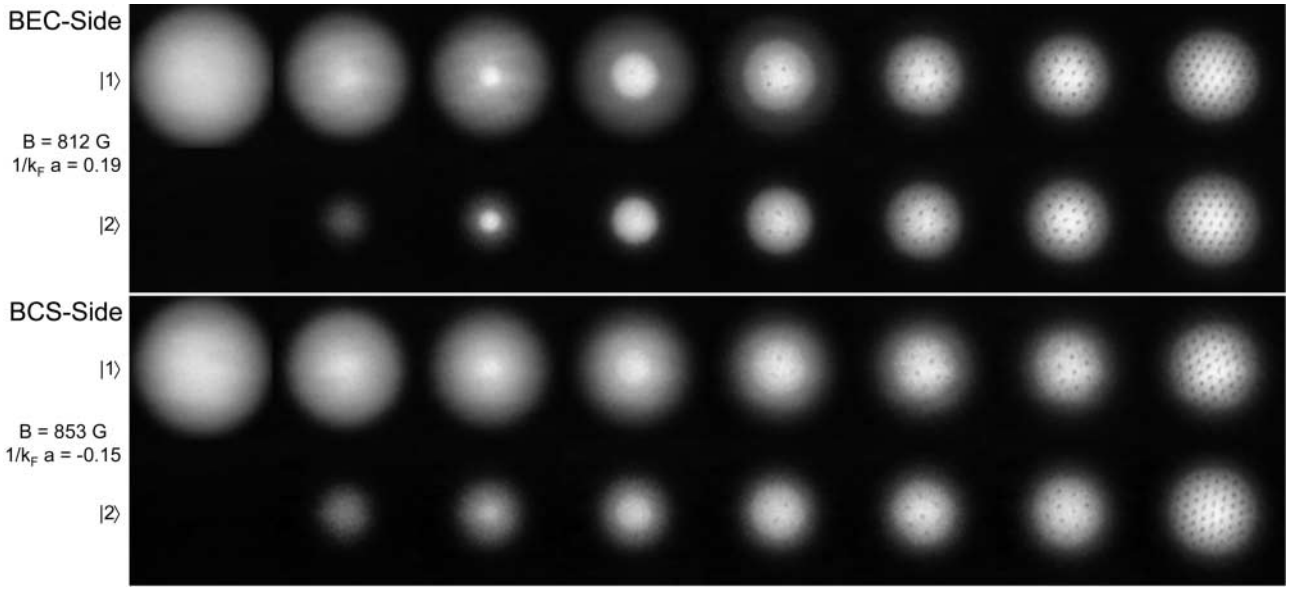

Fig. 1. Superfluidity in a strongly interacting Fermi gas with imbalanced populations. The upper (lower) pair of rows shows clouds prepared at 812 G, on the BEC side (853 G, BCS side), where $1/k_F a = 0.2$ ($1/k_F a = -0.15$). In each pair of rows, the upper image shows state $|1\rangle$, the lower one state $|2\rangle$. For the 812-G data, the population imbalance $\delta = (N_2 - N_1)/(N_1 + N_2)$ between N_1 atoms in state $|1\rangle$ and N_2 in state $|2\rangle$ was (from left to right) 100, 90, 80, 62, 28, 18, 10, and 0%. For the 853-G data, the imbalance was 100, 74, 58, 48, 32, 16, 7, and 0%. For different values of δ, the total number of atoms varied only within 20% around $N = 7 \times 10^6$, with the exception of the end points $\delta = 100\%$ ($N = 1 \times 10^7$) and $\delta = 0\%$ ($N = 1.2 \times 10^7$). The field of view of each image is 1.4 mm by 1.4 mm.

superfluid even for arbitrarily weak interactions, and no phase transition occurs. In the case of unequal mixtures, the phase diagram is predicted to be much richer (*23*–*28*). In the molecular limit of tight binding, all fermions in the less populated spin state will pair up with atoms in the other state. The resulting molecular condensate will spatially coexist with the remaining Fermi sea of unpaired atoms. As the repulsive interaction between atoms and molecules is increased, the condensate will start to expel unpaired atoms, leading to a phase separation of the superfluid from the normal phase (*24*–*26*, *29*, *30*). This picture is expected to extend into the BCS limit of weakly bound pairs, where the pairing gap Δ prevents unpaired atoms from entering the BCS superfluid (*24*–*26*, *31*). As the binding energy and hence the pairing gap is further reduced, Δ will eventually become small compared to the chemical potential difference $\delta\mu = \mu_2 - \mu_1$ between the two spin states, allowing unpaired excess atoms to enter the superfluid region. Close to this point, superfluidity will cease to exist. In the weakly interacting BCS limit, the pairing gap is exponentially small compared to the Fermi energy; hence, an exponentially small population imbalance can destroy superfluidity.

This superfluid-to-normal transition is an example of a quantum phase transition, which occurs even at zero temperature, when all thermal fluctuations are frozen out and only quantum fluctuations prevail. It can also be driven by increasing the mismatch in chemical potentials between the two spin states to the critical value of $\delta\mu \approx \Delta$, inducing collapse into the normal state. In this context the phase transition is known as the Pauli or Clogston limit of superfluidity (*1*). However, its exact nature—whether there is one or several first- and/or second-order transitions—remains the subject of debate (*6*, *27*, *28*).

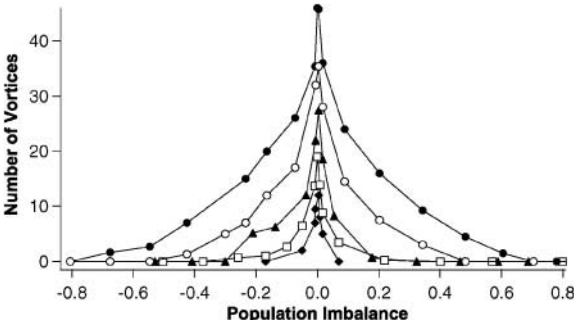

Fig. 2. Vortex number versus population imbalance for different interaction strengths. Results are shown for 812 G or $1/k_Fa = 0.2$ (●), 853 G ($1/k_Fa = -0.15$, ○), 874 G ($1/k_Fa = -0.3$, ▲), 896 G ($1/k_Fa = -0.4$, □), and 917 G ($1/k_Fa = -0.5$, ♦).

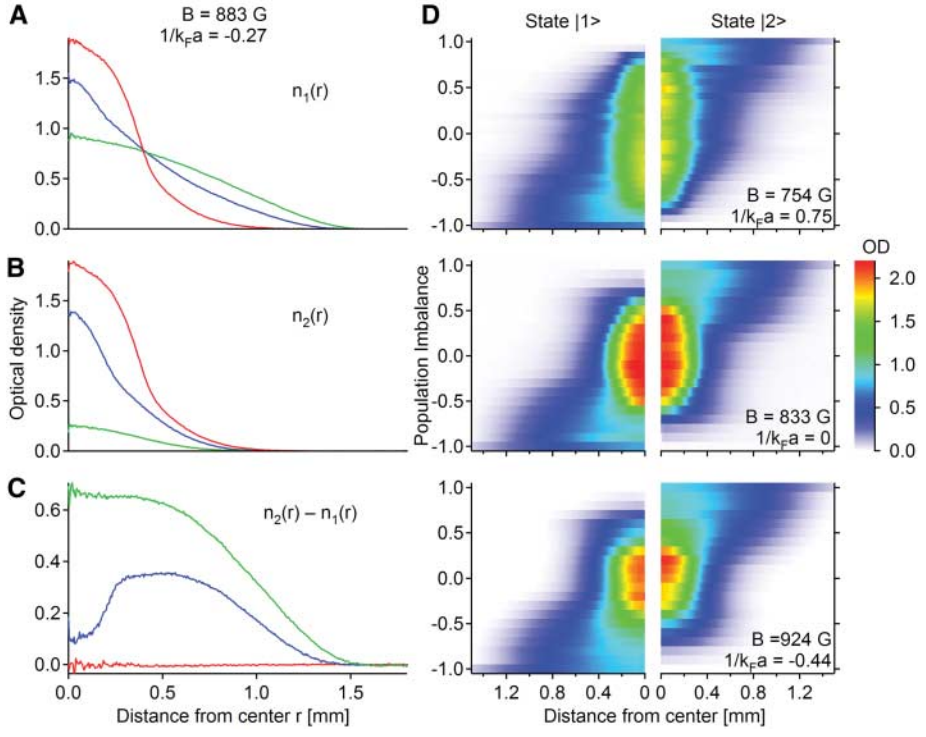

Fig. 3. Radial density profiles of the two components of a strongly interacting Fermi gas mixture with unequal populations. The profiles are azimuthal averages of the axially integrated density. (**A** and **B**) Profiles of the component in state $|1\rangle$ and $|2\rangle$, respectively, originating from 883 G ($1/k_Fa = -0.27$). The imaging procedure, as detailed in the text and in (*32*), involves a magnetic-field sweep and ballistic expansion. The population imbalance was $\delta = 0\%$ (red), $\delta = 46\%$ (blue), and $\delta = 86\%$ (green). (**C**) Difference between the distributions in state $|1\rangle$ and $|2\rangle$. The total number of atoms was $N = 2.3 \times 10^7$. The clear dip in the blue curve caused by the pair condensate indicates phase separation of the superfluid from the normal gas. (**D**) Color-coded profiles of clouds prepared at three different interaction strengths. The condensate is clearly visible as the dense central part surrounded by unpaired fermions or uncondensed molecules. Spin-polarized clouds ($\delta = \pm 100\%$) are not in thermal equilibrium, owing to Pauli suppression of collisions. OD, optical density.

Imbalanced spin populations. As the starting point of our experiments, we prepared a degenerate Fermi gas of spin-polarized ^{6}Li atoms, using methods of laser cooling, sympathetic cooling by sodium atoms, and optical trapping (*32*). A radiofrequency sweep with an adjustable sweep rate created a variable spin mixture of the two lowest hyperfine states, labeled $|1\rangle$ and $|2\rangle$. Interactions between these two states are strongly enhanced around a 300-G-wide Feshbach resonance located at $B_0 = 834$ G. At lower values of the magnetic-bias field B, two isolated fermions can bind into a stable molecule (BEC side), whereas at higher values fermion pairs can exist only in the stabilizing presence of the surrounding gas (BCS side). The interaction is described by the parameter $1/k_Fa$, where a is the scattering length and k_F is defined as the Fermi momentum of a noninteracting, equal spin mixture.

For the study of vortices and superfluid flow as a function of population imbalance, the spin mixture was set in rotation on the BEC side, using two laser beams that rotated symmetrically around the cloud (*19*, *32*). Starting with either a rotating or a nonrotating cloud, we then varied the interaction strength by ramping the magnetic field B to several values around the Feshbach resonance. To image the fermion pair condensates, the cloud was released from the optical trap and the binding energy of the pairs was increased by switching the magnetic field to the BEC side, far away from resonance (*13*, *14*, *19*, *32*). This revealed the center-of-mass wave function of the pairs and thus, for rotating clouds, the eventual presence of vortices.

Figure 1 shows images of the two spin states for varying population imbalance, originating from the BEC side ($B < 834$ G) and from the BCS side ($B > 834$ G) of the resonance. Starting with a pure Fermi sea in state $|1\rangle$, we see how gradually, for increasing numbers in the second spin state $|2\rangle$, first a normal (uncondensed) cloud of fermion pairs emerges, then a condensate peak appears within the normal cloud (see also Fig. 3, A and B). The condensate can be clearly distinguished in the minority cloud as the dense

central region (appearing as white in the image) surrounded by the lower density normal component (appearing as gray). As the condensate size increases and the friction due to the normal component decreases, vortices appear in the rotating cloud, a direct and unambiguous signature of superfluid flow. As expected, the largest condensates with the largest number of vortices are obtained for an equal mixture. However, superfluidity in the strongly interacting Fermi gas is clearly not constrained to a narrow region around the perfectly balanced spin mixture, but is observed for large population asymmetries.

Figures 1 and 2 summarize our findings for rotating spin mixtures and displays the number of detected vortices versus the population imbalance between the two spin states. The vortex number measures qualitatively how deep the system is in the superfluid phase: The higher the nonsuperfluid fraction, the faster the condensate's rotation will damp given the nonvanishing anisotropy $[(\omega_x - \omega_y)/(\omega_x + \omega_y) \approx 1.5\%]$ of our trap (*19*, *33*, *34*). Figure 2 therefore shows the shrinking of the superfluid region with decreasing interaction strength on the BCS side, closing in on the optimal situation of equal populations.

The fraction of condensed fermion pairs. Close to the breakdown of superfluidity, vortices are strongly damped and difficult to observe. Therefore, the presence of vortices provides only a lower bound on the size of the superfluid window. A more detailed map of the superfluid phase as a function of interaction strength and temperature was obtained from a study of condensate fractions, determined from cloud profiles such as those shown in Fig. 3. Throughout the whole crossover region, pair condensation occurred for a broad range of population imbalances. As expected, this range was even wider than that obtained from the observation of vortices.

An intriguing property of the superfluid state with imbalanced populations is the clear depletion in the excess fermions of the majority component (Fig. 3C). The profiles in Fig. 3 present the axially integrated density; hence, the true depletion in the 3D density is even stronger. The condensate seems to repel the excess fermions. This feature was observed after expansion at 690 G, where interactions are still strong (initially $1/k_F a \approx 2.0$). The expansion, at least in the region around the condensate, is hydrodynamic and should proceed as a scaling transformation (*35*, *36*). Therefore, the depletion observed in expansion hints at spatial phase separation of the superfluid from the normal state. This effect was observed throughout the resonance region, and on resonance even when no magnetic field ramps were performed during expansion. After submission of our work, depletion of excess fermions in the center of the trap was reported (*37*). However, to distinguish a phase-separated state with equal densities in the superfluid region from more exotic states allowing unequal densities, a careful analysis of the 3D density, reconstructed from the integrated optical densities, will be necessary.

We did not observe (by simultaneously imaging along the long and short axis) a modulation in the condensate density as would be predicted for the FFLO state (*23*, *38*, *39*). However, this state is predicted to be favored only in a narrow region of parameter space and might have escaped our attention.

The condensate fraction was determined from the minority component, which in all cases is very well fit by a Gaussian for thermal molecules and unpaired atoms, plus a Thomas-Fermi profile for the condensate (fig. S2) (*32*). Figure 4 shows the condensate fraction obtained for varying population difference and temperature, and for several magnetic fields (i.e., interaction strengths) around resonance. The data for 754 G, on the BEC side of the resonance, show condensation over almost the entire range of population imbalance. As the interaction strength is increased toward resonance, the condensate fraction for equal mixtures grows (*14*). However, for large population asymmetries, the condensate disappears. The window of condensation shrinks further as we cross the resonance and move to the BCS side (Fig. 4, 833 to 924 G).

The temperature varied with number imbalance, as indicated in the insets of Fig. 4. The temperature maximum for equal mixtures at 754 G is likely due to the greater energy release when more deeply bound molecules were formed and explains the smaller condensate fraction for equal mixtures found at this field. For higher fields, the temperature changes much less with the spin composition (*32*). The observed critical population imbalance was only weakly dependent on temperature. This may reflect the fact that well below the critical temperature for superfluidity, the pairing gap is only weakly dependent on temperature (*40*). The critical imbalance at our coldest temperatures will thus essentially coincide with its value at zero temperature.

On resonance, where the scattering length a diverges, the system is in the unitary regime (*41*), where the only remaining energy scales of the system are the Fermi energies $E_{F,1}$ and $E_{F,2}$ of the two spin components (*42*). The breakdown of

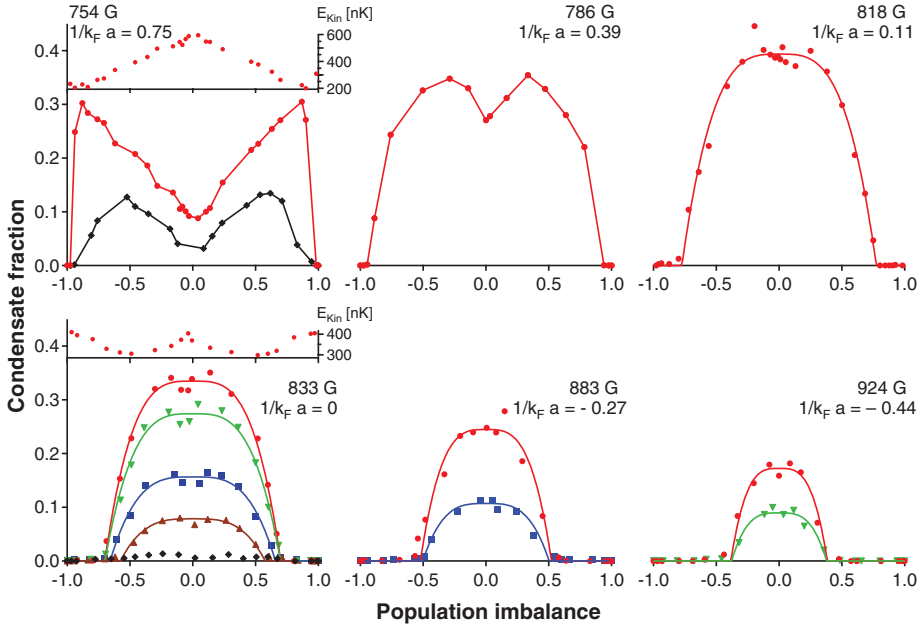

Fig. 4. Condensate fraction versus population imbalance for several temperatures and interaction strengths. The total number of atoms $N = 2.3 \times 10^7$ is constant to within 20% for all data points ($T_F = 1.9\ \mu K$ for an equal mixture) (*32*). For a given population imbalance, the uppermost curves for different magnetic fields are approximately isentropically connected. The different symbols correspond to different evaporation ramps. The average radial kinetic energy per molecule of thermal clouds in the minority component serves as an indicator for temperature and is shown in the insets for 754 G (upper) and 833 G (lower) for the coldest data. On resonance, for a population asymmetry of 50%, we measure an energy of $k_B \times 300$ nK (circles) (k_B is the Boltzmann constant), 345 nK (inverted triangles), 390 nK (squares), 420 nK (triangles), and 505 nK (diamonds). The critical population imbalance δ_c for the breakdown of condensation at 754 G is about $\delta_c^{754} \approx 96\%$, and at 786 G it is $\delta_c^{786} \approx 95\%$. For the data at higher magnetic fields, we determine δ_c through a threshold fit to the first three data points with nonzero condensate fraction for each sign of asymmetry. Although we could have used any reasonable threshold function, empirically, it was found that the function $n_c(1 - |\delta/\delta_c|^{3.3})$ (n_c – maximum condensate fraction) provided a good fit to all data points. Therefore, in the threshold fits and is shown as a guide to the eye.

superfluidity occurs for a certain universal ratio of these two or equivalently, in a harmonic trap, for a certain critical population imbalance. We determine this universal number to be $\delta_c \approx \pm 70(3)\%$ for our approximately harmonic trapping potential. In (*37*), depletion of excess fermions was reported up to an imbalance of 85% and was interpreted as indirect evidence for superfluidity. However, superfluidity was not directly observed, and our data show that the system is normal at this imbalance.

The critical imbalance δ_c corresponds to a Fermi energy difference $\delta E_F = E_{F,2} - E_{F,1} = [(1 + \delta_c)^{1/3} - (1 - \delta_c)^{1/3}]E_F = 0.53(3)E_F$, where E_F is the Fermi energy of an equal mixture of noninteracting fermions. The standard BCS state is predicted (*1*) to break down for a critical chemical-potential difference $\delta\mu = \sqrt{2}\,\Delta$. On resonance, however, Monte-Carlo studies predict (*24*) the superfluid breakdown to occur when $\delta\mu = 2.0(1)\Delta = 1.0(1)E_F$. Only in the weakly interacting regime do the chemical potentials equal the Fermi energies. Quantitative agreement with the Monte-Carlo study would require that $\delta\mu \approx 2\delta E_F$. This is not unreasonable given that interactions will reduce the chemical potential of the minority component. In a preliminary analysis, we indeed find close agreement with theory.

Figure 5 summarizes our findings, showing the critical mismatch in Fermi energies for which we observed the breakdown of superfluidity as well as the pairing gap Δ versus the interaction parameter $1/k_F a$. Far on the BEC side of the resonance, the superfluid is very robust with respect to population imbalance. Here, pairing is dominantly a two-body process: The smallest cloud of atoms in state $|1\rangle$ will fully pair with atoms in state $|2\rangle$ and condense at sufficiently low temperatures. On the BCS side of the resonance, however, pairing is purely a many-body effect and depends on the density of the two Fermi clouds. As the density of the minority component becomes smaller, the net energy gain from forming a pair condensate will decrease. Even at zero temperature, this eventually leads to the breakdown of superfluidity and the quantum phase transition to the normal state. We have experimentally confirmed the qualitative picture that fermionic superfluidity breaks down when the difference in chemical potentials between the two species becomes larger than the pairing gap.

Concluding remarks and outlook. We have observed superfluidity with imbalanced spin populations. Contrary to expectations for the weakly interacting case, superfluidity in the resonant region is extremely stable against population imbalance. As the asymmetry is increased, we observe the quantum phase transition to the normal state, known as the Pauli limit of superfluidity. Our observation opens up intriguing possibilities for further studies on Fermi systems with mismatched Fermi surfaces. One important aspect concerns the density distribution in the superfluid regime. Standard BCS theory allows only equal spin densities, which would entail complete phase separation of the superfluid from the normal density. More exotic solutions (*6*) allow superfluidity also with imbalanced densities, most notably the FFLO state. A more detailed scan of the parameter space and precise measurements of spatial profiles might resolve the long-standing question of the true ground state. Equally fascinating is the nature of the strongly correlated normal state slightly below resonance. For sufficient population imbalance, we have the remarkable situation in which bosonic molecules, stable even in isolation, do not condense at zero temperature, owing to the presence of the Fermi sea.

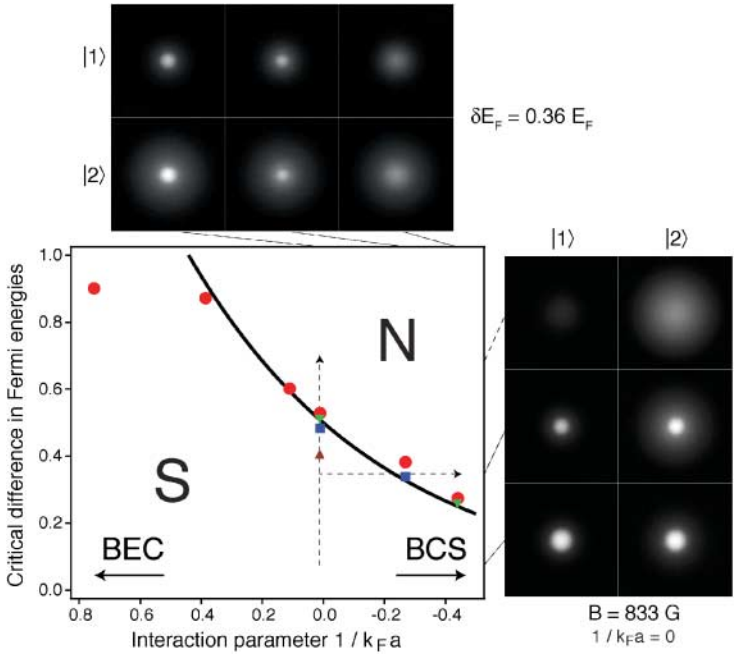

Fig. 5. Critical difference in Fermi energies δE_F between the two spin states for which the superfluid-to-normal transition is observed. δE_F for each interaction strength and temperature is obtained from the critical population imbalance determined in Fig. 3 using $\delta E_F/E_F = (1 + \delta_c)^{1/3} - (1 - \delta_c)^{1/3}$. The symbols are defined in Fig. 3. The line shows the expected variation of the pairing gap Δ, where the value on resonance has been taken from (*24*) and the exponential behavior in the BCS regime, $\Delta \sim e^{-\pi/2k_F|a|}$, was assumed. Although the trend of δE_F is expected to follow that of Δ, the close agreement is coincidental. Representative density profiles illustrate the quantum phase transition for fixed interaction and for fixed population imbalance along the dashed lines.

References and Notes

1. A. M. Clogston, *Phys. Rev. Lett.* **9**, 266 (1962).
2. P. Fulde, R. A. Ferrell, *Phys. Rev.* **135**, A550 (1964).
3. A. J. Larkin, Y. N. Ovchinnikov, *Zh. Eksp. Teor. Fiz.* **47**, 1136 (1964) [*Sov. Phys. JETP* **20**, 762 (1965)].
4. G. Sarma, *J. Phys. Chem. Solids* **24**, 1029 (1963).
5. W. V. Liu, F. Wilczek, *Phys. Rev. Lett.* **90**, 047002 (2003).
6. R. Casalbuoni, G. Nardulli, *Rev. Mod. Phys.* **76**, 263 (2004).
7. H. A. Radovan *et al.*, *Nature* **425**, 51 (2003).
8. A. Bianchi, R. Movshovich, C. Capan, P. G. Pagliuso, J. L. Sarrao, *Phys. Rev. Lett.* **91**, 187004 (2003).
9. D. Vollhardt, P. Wölfle, *The Superfluid Phases of Helium 3* (Taylor & Francis, London, 1990).
10. C. A. Regal, C. Ticknor, J. L. Bohn, D. S. Jin, *Nature* **424**, 47 (2003).
11. S. Jochim *et al.*, *Science* **302**, 2101 (2003).
12. M. W. Zwierlein *et al.*, *Phys. Rev. Lett.* **91**, 250401 (2003).
13. C. A. Regal, M. Greiner, D. S. Jin, *Phys. Rev. Lett.* **92**, 040403 (2004).
14. M. W. Zwierlein *et al.*, *Phys. Rev. Lett.* **92**, 120403 (2004).
15. T. Bourdel *et al.*, *Phys. Rev. Lett.* **93**, 050401 (2004).
16. J. Kinast, S. L. Hemmer, M. E. Gehm, A. Turlapov, J. E. Thomas, *Phys. Rev. Lett.* **92**, 150402 (2004).
17. C. Chin *et al.*, *Science* **305**, 1128 (2004).
18. G. B. Partridge, K. E. Strecker, R. I. Kamar, M. W. Jack, R. G. Hulet, *Phys. Rev. Lett.* **95**, 020404 (2005).
19. M. W. Zwierlein, J. R. Abo-Shaeer, A. Schirotzek, C. H. Schunck, W. Ketterle, *Nature* **435**, 1047 (2005).
20. D. M. Eagles, *Phys. Rev.* **186**, 456 (1969).
21. A. J. Leggett, in *Modern Trends in the Theory of Condensed Matter. Proceedings of the XVIth Karpacz Winter School of Theoretical Physics, Karpacz, Poland, 1980* (Springer-Verlag, Berlin, Karpacz, Poland, 1980), pp. 13–27.
22. P. Nozières, S. Schmitt-Rink, *J. Low Temp. Phys.* **59**, 195 (1985).
23. A. Sedrakian, J. Mur-Petit, A. Polls, H. Müther, *Phys. Rev. A.* **72**, 013613 (2005).
24. J. Carlson, S. Reddy, *Phys. Rev. Lett.* **95**, 060401 (2005).
25. C.-H. Pao, S.-T. Wu, S.-K. Yip, preprint available at http://xxx.lanl.gov/abs/cond-mat/0506437.
26. D. E. Sheehy, L. Radzihovsky, preprint available at http://xxx.lanl.gov/abs/cond-mat/0508430.
27. D. T. Son, M. A. Stephanov, preprint available at http://xxx.lanl.gov/abs/cond-mat/0507586.
28. K. Yang, preprint available at http://xxx.lanl.gov/abs/cond-mat/0508484.
29. L. Viverit, C. J. Pethick, H. Smith, *Phys. Rev. A.* **61**, 053605 (2000).
30. S. Powell, S. Sachdev, H. P. Büchler, *Phys. Rev. B* **72**, 024534 (2005).
31. P. F. Bedaque, H. Caldas, G. Rupak, *Phys. Rev. Lett.* **91**, 247002 (2003).

32. Materials and methods are available as supporting material on *Science* Online.
33. J. R. Abo-Shaeer, C. Raman, W. Ketterle, *Phys. Rev. Lett.* **88**, 070409 (2002).
34. D. Guéry-Odelin, *Phys. Rev. A.* **62**, 033607 (2000).
35. Y. Kagan, E. L. Surkov, G. V. Shlyapnikov, *Phys. Rev. A.* **55**, R18 (1997).
36. C. Menotti, P. Pedri, S. Stringari, *Phys. Rev. Lett.* **89**, 250402 (2002).
37. G. B. Partridge, W. Li, R. I. Kamar, Y.-a. Liao, R. G. Hulet, *Science*, **311**, 503 (2006); published online 22 December 2005 (10.1126/science.1122876).
38. T. Mizushima, K. Machida, M. Ichioka, *Phys. Rev. Lett.* **94**, 060404 (2005).
39. P. Castorina, M. Grasso, M. Oertel, M. Urban, D. Zappalà, *Phys. Rev. A.* **72**, 025601 (2005).
40. A. A. Abrikosov, L. P. Gorkov, I. E. Dzyaloshinski, *Methods of Quantum Field Theory in Statistical Physics* (Dover, New York, 1975).
41. G. Bertsch, INT Workshop on Effective Field Theory in Nuclear Physics (Seattle, WA, February 1999).
42. T. D. Cohen, *Phys. Rev. Lett.* **95**, 120403 (2005).
43. We thank G. Campbell for critical reading of the manuscript and X.-G. Wen, E. Demler, and S. Sachdev for stimulating discussions. This work was supported by the NSF, Office of Naval Research, Army Research Office, and NASA.

Supporting Online Material
www.sciencemag.org/cgi/content/full/1122318/DC1
Materials and Methods
Figs. S1 and S2
References and Notes

7 November 2005; accepted 14 December 2005
Published online 22 December 2005;
10.1126/science.1122318
Include this information when citing this paper.

Community Genomics Among Stratified Microbial Assemblages in the Ocean's Interior

Edward F. DeLong,[1]* Christina M. Preston,[2] Tracy Mincer,[1] Virginia Rich,[1] Steven J. Hallam,[1] Niels-Ulrik Frigaard,[1] Asuncion Martinez,[1] Matthew B. Sullivan,[1] Robert Edwards,[3] Beltran Rodriguez Brito,[3] Sallie W. Chisholm,[1] David M. Karl[4]

Microbial life predominates in the ocean, yet little is known about its genomic variability, especially along the depth continuum. We report here genomic analyses of planktonic microbial communities in the North Pacific Subtropical Gyre, from the ocean's surface to near–sea floor depths. Sequence variation in microbial community genes reflected vertical zonation of taxonomic groups, functional gene repertoires, and metabolic potential. The distributional patterns of microbial genes suggested depth-variable community trends in carbon and energy metabolism, attachment and motility, gene mobility, and host-viral interactions. Comparative genomic analyses of stratified microbial communities have the potential to provide significant insight into higher-order community organization and dynamics.

Microbial plankton are centrally involved in fluxes of energy and matter in the sea, yet their vertical distribution and functional variability in the ocean's interior is still only poorly known. In contrast, the vertical zonation of eukaryotic phytoplankton and zooplankton in the ocean's water column has been well documented for over a century (*1*). In the photic zone, steep gradients of light quality and intensity, temperature, and macronutrient and trace-metal concentrations all influence species distributions in the water column (*2*). At greater depths, low temperature, increasing hydrostatic pressure, the disappearance of light, and dwindling energy supplies largely determine vertical stratification of oceanic biota.

For a few prokaryotic groups, vertical distributions and depth-variable physiological properties are becoming known. Genotypic and phenotypic properties of stratified *Prochlorococcus* "ecotypes" for example, are suggestive of depth-variable adaptation to light intensity and nutrient availability (*3*–*5*). In the abyss, the vertical zonation of deep-sea piezophilic bacteria can be explained in part by their obligate growth requirement for elevated hydrostatic pressures (*6*). In addition, recent cultivation-independent (*7*–*15*) surveys have shown vertical zonation patterns among specific groups of planktonic *Bacteria*, *Archaea*, and *Eukarya*. Despite recent progress however, a comprehensive description of the biological properties and vertical distributions of planktonic microbial species is far from complete.

Cultivation-independent genomic surveys represent a potentially useful approach for characterizing natural microbial assemblages (*16*, *17*). "Shotgun" sequencing and whole genome assembly from mixed microbial assemblages has been attempted in several environments, with varying success (*18*, *19*). In addition, Tringe *et al*. (*20*) compared shotgun sequences of several disparate microbial assemblages to identify community-specific patterns in gene distributions. Metabolic reconstruction has also been attempted with environmental genomic approaches (*21*). Nevertheless, integrated genomic surveys of microbial communities along well-defined environmental gradients (such as the ocean's water column) have not been reported.

To provide genomic perspective on microbial biology in the ocean's vertical dimension, we cloned large [~36 kilobase pairs (kbp)] DNA fragments from microbial communities at different depths in the North Pacific Subtropical Gyre (NPSG) at the open-ocean time-series station ALOHA (*22*). The vertical distribution of microbial genes from the ocean's surface to abyssal depths was determined by shotgun sequencing of fosmid clone termini. Applying identical collection, cloning, and sequencing strategies at seven depths (ranging from 10 m to 4000 m), we archived large-insert genomic libraries from each depth-stratified microbial community. Bidirectional DNA sequencing of fosmid clones (~10,000 sequences per depth) and comparative sequence analyses were used to identify taxa, genes, and metabolic pathways that characterized vertically stratified microbial assemblages in the water column.

Study Site and Sampling Strategy

Our sampling site, Hawaii Ocean Time-series (HOT) station ALOHA (22°45' N, 158°W), represents one of the most comprehensively characterized sites in the global ocean and has been a focal point for time series–oriented oceanographic studies since 1988 (*22*). HOT investigators have produced high-quality spatial and time-series measurements of the defining physical, chemical, and biological oceanographic parameters from surface waters to the seafloor. These detailed spatial and temporal datasets present unique opportunities for placing microbial genomic depth profiles into appropriate oceanographic context (*22*–*24*) and leverage these data to formulate meaningful ecological hypotheses. Sample depths were selected, on the basis of well-defined physical, chemical, and biotic characteristics, to represent discrete zones in the water column (Tables 1 and 2, Fig. 1; figs. S1 and S2). Specifically, seawater samples from the upper euphotic zone (10 m and 70 m), the base of the chlorophyll maximum (130 m), below the base of the euphotic zone (200 m), well below the upper mesopelagic (500 m), in the core of the dissolved oxygen minimum layer (770 m), and in the deep abyss, 750 m above the seafloor (4000 m), were collected for preparing microbial community DNA libraries (Tables 1 and 2, Fig. 1; figs. S1 and S2).

The depth variability of gene distributions was examined by random, bidirectional end-sequencing of ~5000 fosmids from each depth, yielding ~64 Mbp of DNA sequence total from the 4.5 Gbp archive (Table 1). This represents raw sequence coverage of about 5 (1.8 Mbp sized) genome equivalents per depth. Because we surveyed ~180 Mbp of cloned DNA (5000 clones by

[1]Massachusetts Institute of Technology, Cambridge, MA 02139, USA. [2]Monterey Bay Aquarium Research Institute, Moss Landing, CA 95064, USA. [3]San Diego State University, San Diego, CA 92182, USA. [4]University of Hawaii Honolulu, HI 96822, USA.

*To whom correspondence should be addressed. E-mail: delong@mit.edu